First-principles calculations on slip system activation in the rock salt structure: Electronic origin of ductility in silver chloride

Atsutomo Nakamura[1, *], Masaya Ukita[1], Naofumi Shimoda[1], Yuho Furushima[1], Kazuaki Toyoura[2] and Katsuyuki Matsunaga[1, 3]

[1] Department of Materials Science and Engineering, Nagoya University, Furo-cho, Chikusa, Nagoya 464-8603, Japan.

[2] Department of Materials Science and Engineering, Kyoto University, Yoshida-Honmachi, Sakyo, Kyoto 606-8501, Japan.

[3] Nanostructures Research Laboratory, Japan Fine Ceramics Center, 2-4-1 Mutsuno, Atsuta, Nagoya 456-8587, Japan.

*Corresponding author: Atsutomo Nakamura

Department of Materials Science and Engineering, Nagoya University,

Furo-cho, Chikusa-ku, Nagoya 464-8603, Japan

Tel: +81-52-789-3366, Fax: +81-52-789-3366

Email: nakamura@numse.nagoya-u.ac.jp

(Current e-mail address: anaka@nagoya-u.jp)

Abstract

First-principles calculations were performed to understand an electronic origin of high ductility in silver chloride (AgCl) with the rock salt structure. From calculations of generalized stacking fault (GSF) energies for different slip systems, it was found that only the {110}<1$\bar{1}$0> slip system is favorably activated in sodium chloride (NaCl) with the same rock salt structure whereas AgCl shows three kinds of possible slip systems along the <1$\bar{1}$0> direction on the {001}, {110}, and {111} planes, which is in excellent agreement with experiment. Detailed analyses of the electronic structures across slip planes showed that the more covalent character of bonding of Ag-Cl than Na-Cl tends to make the slip motion energetically favorable. It was also surprising to find out that strong Ag-Ag covalent bonds across the slip plane are formed in the {001}<110> slip system in AgCl, which makes it possible to activate the multiple slip systems in AgCl.

Keywords: plasticity of crystals; ionic crystals; first-principles calculations; generalized stacking fault (GSF); crystal orbital Hamilton population (COHP)

1. Introduction

Ionic crystals are generally brittle at low temperatures because slip systems to be activated are limited by electrostatic interactions between ions. In the case of alkali halides with the rock salt structure such as sodium chloride (NaCl), for example, only the {110}<1$\bar{1}$0> slip system can be activated when they are deformed at room temperature [1-2]. The {001} plane of the rock salt structure is the closest packed atomic plane, and thus the {001}<110> system is expected to be activated. Nevertheless, activation of the {001}<110> system is difficult in actuality because this system forces like ions to be nearer neighbors. In addition, since the {001} plane has a relatively small surface energy, cleavage is easy to occur along this plane [2-3]. Cleavage on the {001} plane is also ascribed to electrostatic repulsion between like ions.

In contrast, silver halide crystals such as silver chloride (AgCl) with the same rock salt structure exhibit more ductile mechanical properties than alkali halides [2, 4-6]. It was reported that the slip systems along the {111} and {001} planes as well as along the {110} plane in AgCl are activated even at low temperatures [5-6]. This is a striking difference from that in NaCl. It was also found that cleavage on the {001} plane does not occur in AgCl. Since AgCl and NaCl have the same crystal structure and almost the same lattice parameters (a = 0.55 nm in AgCl, a = 0.56 nm in NaCl), such differences in slip deformation cannot be explained from a simple ionic nature of bonding or a crystallographic viewpoint. However, a physical origin on activation of multiple slip systems and the associated ductility in AgCl has been poorly understood so far.

In this study, first-principles calculations were performed to understand activation of multiple slip systems in AgCl at electronic and atomic levels. Since dislocation motion in a crystal is not easy to be dealt with in a first-principles manner due to demanding computational costs, an alternative approach of the generalized stacking fault (GSF) energy (Γ surface) [7] was employed to investigate available slip systems in the rock salt structure. Effectiveness of GSF energies for studies of possible slip systems can also be seen from the recent paper by De Leon *et al*., where the different slip systems at low temperatures in metal carbides can be explained from differences in GSF energies and the associated bonding characters across the

slip planes [8]. Unlike metallic and covalent systems, dislocations in ionic crystals might suffer charge effects at the cores [1]. Although GSF does not directly deal with dislocations cores and core charges, the GSF profiles reflect distorted atomic arrangements across the slip planes and their energies, as found in real dislocation cores, which might suggest possible applicability of GSF even for ionic crystals. Evaluation of GSF energies is not only useful to investigate activation of particular slip systems, but also can provide the Peierls stresses combined with the Peierls-Nabarro (PN) equation [9-10]. In order to quantitatively evaluate bonding states during slip in the present systems, the crystal orbital Hamilton population (COHP) analyses [11] were performed. Specific chemical bonds to realize the multiple slip systems of AgCl were discussed.

2. Computational methodology

First-principles calculations in this study were based on the projector augmented wave (PAW) method as implemented in the VASP code [12-13]. In the PAW potentials, Na 3*s*, Ag 4*d*5*s* and Cl 3*s*3*p* electrons were treated as valence electrons. The generalized gradient approximation (GGA) parameterized by Perdew, Burke, and Ernzerhof was used for the exchange-correlation terms [14], and wavefunctions were expanded by plane waves with a cut-off energy of 350 eV.

Figure 1 displays slip systems in the rock salt structure that were considered to calculate GSF energies. The *p* corresponds to normal vectors of individual slip planes of {001}, {110}, and {111}. Light blue solid arrows in the figure also correspond to individual slip directions of <100> and <110>. In addition, the slip direction of $<2\bar{1}\bar{1}>$ on the {111} plane, denoted by the light blue open arrow, is also considered. This is because Suzuki and Takeuchi previously suggested that ductility of AgCl may be related to slip deformation by the $\{111\}<1\bar{1}0>$ system, where the dislocation could be dissociated into two Shockley partial dislocations of $\vec{b}$ = 1/6$<2\bar{1}\bar{1}>$ and $\vec{b}$ = 1/6$<1\bar{2}1>$ with a low-energy stacking fault. The partials with smaller Burgers vector can facilitate more dislocation motion, namely, more slip deformation.

In order to investigate which slip system can be easily activated in NaCl and AgCl from first-principles calculations, slab models were generated, and ions in a half of atomic layers in

a slab model were rigidly translated by a displacement $u/|\vec{b}|$ toward a particular direction on a particular crystal plane. $|\vec{b}|$ means a size of a minimum translational vector corresponding to the Burgers vector for the slip system being considered. Slab models for slip motion along the {001} and {110} planes included 16 atomic layers in total, which correspond to 8×*p* in Fig.1 (a) and 1(b). Then the numbers of atoms in the supercells for the {001}<100> and {001}<110> systems were 64 and 32, respectively. The slab models were separated by vacuum layers with a thickness of 15 Å in the supercells. An advantage of the supercells with vacuum layers is that atomic relaxation can be done without changing the supercell shape. At individual translations of $u/|\vec{b}|$, all atoms were allowed to relax only perpendicular to the slip planes. Structure optimization was truncated when residual atomic force components (normal to the slip planes) became less than 0.01 eV/Å. GSF energies at given $u/|\vec{b}|$ were obtained by total-energy differences from that at $u/|\vec{b}|$= 0.0 divided by a cross section. Surface energies along {001} and {110} were also calculated for a simple comparison with the GSF energies.

In contrast, a vacuum layer was not introduced into supercells for slip motion along the {111} plane, because a {111} atomic layer consists of like ions and thus the slab models have polar surfaces. In this case, supercells involving 72 atomic layers perpendicular to {111}, which correspond to 12×*p* in Fig.1 (c), were generated. For the {111}<1$\bar{1}$0> and the {111}<2$\bar{1}\bar{1}$> slips, the supercells were considered to consist of three slabs with 24 atomic layers each and to contain three stacking fault planes between the slabs. This is because the atomic configuration for the {111}<2$\bar{1}\bar{1}$> slip is problematic. As will be seen in Fig. 4(a), the [2$\bar{1}\bar{1}$] direction does not have a mirror symmetry. In other words, the [2$\bar{1}\bar{1}$] and [$\bar{2}$11] directions are not crystallographically equivalent. Then, if two stacking fault planes (namely two slabs) were introduced in the supercells to keep the periodic boundary condition (as often seen in the standard supercell technique for grain boundaries), relative displacements of the two slabs toward the [2$\bar{1}\bar{1}$] direction would result in formation of two different stacking faults in the supercells. However, when the supercells with three slabs are used and the three slabs are relatively displaced by a same amount toward the different <2$\bar{1}\bar{1}$> directions of [2$\bar{1}\bar{1}$], [$\bar{1}$2$\bar{1}$] and [$\bar{1}\bar{1}$2], the three stacking fault planes then produced in the supercells are equivalent to one another. This is why such

elongated supercells were employed for the {111} slip in the present study. The thickness of each slab (24 atomic layers) was determined to guarantee the same computational accuracy with those for the other slip systems. It is noted that GSF energies for the {111}<1$\bar{1}$0> and {111}<2$\bar{1}\bar{1}$> slips were obtained from total energy differences divided by a factor of three, due to the three equivalent stacking fault planes involved in the supercells.

Brillion zone integration was performed with a 4×4×4 *k*-point mesh for the unit cell of Fig. 1(a). It is noted that the 4×4×4 *k*-point mesh ensures a good accuracy of the total energy within 1 meV / atom, according to test calculations with more severe *k*-point mesh (8×8×8). In the case of the supercells, *k*-point meshes were selected so as to keep the same *k*-point density with the 4×4×4 one for the unit cell. For example, a 6×4×1 and a 6×6×1 mesh were employed for the supercells with respect to the {110}<1$\bar{1}$0> and {001}<110> slip systems, respectively. It was confirmed that such *k*-point sampling for the supercells provides good convergence of GSF energies less than 0.01 J/m^2.

In order to analyze electronic structures during slip motion in detail, the projected Crystal Orbital Hamilton Population (COHP) analyses were performed [11, 15]. The COHP is obtained by projection of electronic wavefunctions described by plane waves into atomic orbital components. The LOBSTER code was used to calculate the values of COHP with VASP code, which was developed by Mainz et al [16]. As a definition of the present study, a minus value of projected COHP (–pCOHP) was used, where a positive "–pCOHP" indicates a bonding character of atomic orbitals, while a negative value of "–pCOHP" means an antibonding character between atomic orbitals. Summation of –pCOHP values over all electron-occupied wavefunctions in a valence band gives the integrated –pCOHP (–IpCOHP), which means a measure of strength of bonding or antibonding interactions of a particular atomic pair. In the COHP analysis, the grid for *k*-point sampling was set to be the same as that for the GSF energy.

3. Results and discussion

3.1 GSF energies and Peierls stresses for perfect slip in NaCl

Figure 2 (a) and 2(b) show the calculated GSF energies along {001}, {110} and {111} in

NaCl as a function of displacement $u/|\vec{b}|$ along <100> and <110>, respectively. It can be seen that the GSF energies generally increase up to the maximum at $u/|\vec{b}|$ = 0.5 and inversely decrease to its initial state at $u/|\vec{b}|$ = 1.0. Due to the crystallographic periodicity, the GSF energies show symmetric profiles centered at $u/|\vec{b}|$ = 0.5. The dashed horizontal lines display doubles of the calculated surface energies for {001} and {110} ($2\gamma_{s\{001\}}$ and $2\gamma_{s\{110\}}$) as a reference. It is noted that these surface energies are in excellent agreement with the calculated values in the previous papers [17, 18].

As can be seen from Fig. 2(a), the GSF energies of the {001}<100> and {110}<001> systems go beyond the $2\gamma_s$ before $u/|\vec{b}|$ reaches to 0.5. This indicates that the displacements are unstable and energetically favor formation of the two surfaces in the calculation. In fact, it was observed in the present calculations that the slab models for the above slip systems are fully separated into two by shear displacements. In such cases, GSF energies are not plotted in the figures and the data are limited. It is thought, therefore, that the {001}<100> and {110}<001> systems cannot be activated in NaCl. In the cases of slip systems along the <110> direction (see Fig. 2(b)), the {110}<1 $\bar{1}$ 0> system has the smaller GSF energy than {111}<1 $\bar{1}$ 0> and {001}<110>, and also exhibits the smaller values than even $2\gamma_s$ of the {001} plane over the entire range of $u/|\vec{b}|$. It can be said, therefore, that the {110}<1$\bar{1}$0> slip system can be stably activated in NaCl, which is in good agreement with the experimental knowledge on the primary slip system of NaCl. It should be noted here that the GSF energy of {111}<1$\bar{1}$0> becomes almost twice larger than that of {110}<1$\bar{1}$0> at around $u/|\vec{b}|$ = 0.5. This indicates that the {111}<1$\bar{1}$0> system is much more difficult to be activated than {110}<1$\bar{1}$0>. It should be mentioned here that shapes of the GSF energy curves on {110} are in good agreement with those in the former research on NaCl [19].

Peierls stresses in the slip systems were also estimated from the GSF energies according to the methodology proposed by Joós *et al* [20] (Table 1). The estimated Peierls stresses for 1/2<1 $\bar{1}$0> edge dislocations on {111} and {110} in NaCl were $7.2\times10^{-2}\ \mu$ and $9.9\times10^{-3}\ \mu$, respectively, where μ is the shear modulus. Here the elastic constants of μ = 14.6 GPa and the Poisson ratio, ν = 0.247 for NaCl, which were obtained using the method by Liu *et al* [19], were used. It can

be said from the Peierls stresses that the {110}<1$\bar{1}$0> slip system is more easily activated, which can be the single primary slip system at low temperatures in NaCl.

3.2 GSF energies and Peierls stresses for perfect slip in AgCl

Figure 3 shows the calculated GSF energies for AgCl. The dashed lines also display doubles of the calculated surface energies for {001} and {110} ($2\gamma_s${001} and $2\gamma_s${110}). In the similar way to the case in NaCl, the GSF energies for the <100> direction (Fig. 3(a)) readily become larger than $2\gamma_s$ with increasing $u/|\vec{b}|$. These slip systems are expected not to be activated in AgCl.

In contrast, the GSF energies along the <110> direction on the three different planes are much lower than those in NaCl and still lower than the $2\gamma_{s\{110\}}$ and $2\gamma_{s\{001\}}$ (Fig. 3(b)). It can be said that the slip motions on the {110}, {111}, and {001} planes are energetically more favorable. This tendency is in excellent agreement with experimental facts that AgCl has multiple slip systems on these planes along the <110> direction [2, 4-6]. Peierls stresses for 1/2<110> edge dislocations on {001}, {111} and {110} in AgCl were estimated to be 2.7×10^{-2} μ, 1.8×10^{-2} μ and 3.7×10^{-3} μ, respectively (see Table 1), where the elastic constants of μ = 7.00 GPa and ν = 0.434 were used [21]. Therefore, the {110}<1$\bar{1}$0> slip system having the minimum Peierls stress is the easiest slip system to be activated, and the {111}<1$\bar{1}$0> and {001}<110> systems with the second and third smallest Peierls stresses can also be activated at conditions of higher temperatures or larger applied stresses [2, 6, 22].

It is noteworthy to mention here that the GSF profile for the {110}<1$\bar{1}$0> system shows a local minimum at $u/|\vec{b}|$ = 0.5. Since the system is temporarily stabilized by the half of shear displacement, this is an indication that the 1/2<1$\bar{1}$0> edge dislocations on the {110} plane may be dissociated into two equivalent partial dislocations of 1/4<1$\bar{1}$0> with a low-energy stacking fault. The stacking fault energy corresponds to the GSF energy at $u/|\vec{b}|$ = 0.5. Such dissociation makes the individual Burgers vectors smaller than that of the perfect dislocation, and it is thus expected that motion of dislocations in the {110}<1 $\bar{1}$ 0> system is more enhanced by dissociation against applied stresses. Since the GSF profile for NaCl does not have local minima,

the dislocation dissociation may not occur in NaCl, which should also be closely related to more ductility of AgCl than NaCl.

3.3 GSF energies for partial slip on {111} in NaCl and AgCl

Concerning the {111}<1$\bar{1}$0> slip system in AgCl, Suzuki and Takeuchi [2] suggested a possibility that the perfect dislocation of $\vec{b}$ =1/2<1$\bar{1}$0> is dissociated into two Shockley partial dislocations of $\vec{b}$ =1/6<2$\bar{1}\bar{1}$> and $\vec{b}$ = 1/6<1$\bar{2}$1> as shown in Fig. 4(a). This situation is analogous to that in fcc metals. In order to investigate this issue, the GSF energies of the {111}<2$\bar{1}\bar{1}$> slip in NaCl and AgCl were also calculated and compared with those of {111}<1$\bar{1}$0>.

Figure 4(b) shows the GSF energies of the {111}<2$\bar{1}\bar{1}$> slip in NaCl together with those of {111}<1$\bar{1}$0>. Here, not the $u/|\vec{b}|$ but the distance is employed as the horizontal axis in the figure, because the $|\vec{b}|$ in {111}<2$\bar{1}\bar{1}$> has a different length from $|\vec{b}|$ in {111}<1$\bar{1}$0>. Additionally, "A", "B" and "C" in the figure correspond to the individual denoted positions in Fig. 4(a). It was found that the GSF energy at "A" is much lower than that at $u/|\vec{b}|$ = 0.5 for {111}<1$\bar{1}$0>. It is thought, therefore, that slip motion by the Shockley partial should be favorable on {111} in NaCl. It is also noteworthy that the GSF energy at "A" (0.20 J/m^2) is still higher than that of {110}<1$\bar{1}$0> in Fig. 2(b) (0.18 J/m^2). This is in good agreement with the fact that slip deformation on {111} can be activated only at high temperatures. It can be said, therefore, that {111}<1$\bar{1}$0> is not the easiest slip system but can be activated at high temperatures due to dissociation into 1/6<2$\bar{1}\bar{1}$> Shockley partials.

Figure 4(c) shows the GSF energies of the {111}<2$\bar{1}\bar{1}$> slip in AgCl together with those of {111}<1$\bar{1}$0>. It is remarkable that the energies are not much changed around the displacements from "A" to "B". It was also found that the GSF energy at "A" takes slightly lower values than that at $u/|\vec{b}|$ = 0.5 in {111}<1$\bar{1}$0>. This means that the Shockley partial slip is possible on {111}. However, since the difference between these slip routes is small, it is thought that the perfect slip of {111}<1$\bar{1}$0> should be also possible in AgCl. It is known in experiment that the shape of slip lines in deformed AgCl is sensitive to the deformation temperature, which suggests that

whether the dislocations on {111} are perfect or partial depends on the temperature [2]. This can also be understood from the present result that perfect slip and partial slip on {111} provide similar GSF barriers for slip motion. Meanwhile, the GSF energy at "A" in AgCl is much higher than that of {110}<1$\bar{1}$0> in Fig. 3(b). Therefore, {110}<1$\bar{1}$0> is still the easiest slip system in AgCl.

3.4 Electronic structures of undeformed NaCl and AgCl

As stated above, GSF energies well reproduce the overall trend in available slip systems at low temperatures in NaCl and AgCl. The major difference between NaCl and AgCl is that the {111}<1$\bar{1}$0> and {001}<110> systems as well as {110}<1$\bar{1}$0> can be activated in AgCl. In order to explain such a difference, it would be beneficial to understand fundamental characteristics of electronic structures of NaCl and AgCl before deformation.

Figure 5 shows densities of states (DOSs) and –pCOHPs profiles for NaCl and AgCl without shear displacement (perfect crystals). Energy bands below 0 eV indicate electron-occupied ones. As can be seen, the valence band of NaCl is mainly composed of Cl-3*p* orbitals, and outermost Na-3*s* and Na-3*p* orbitals mainly forming the conduction band have minor contribution to the valence band. The admixture between Na-3*sp* and Cl-3*p* orbitals at the lower-energy peak around –2 eV contributes to a small covalent nature of Na-Cl bonding. The band gap is more than 4 eV, and such a large band gap as well as the slight atomic-orbital overlap are typical in ionically bonded systems.

In contrast, the valence band of AgCl includes Ag-4*d* orbitals forming the most prominent peaks at around –2 eV. Ag^+ has an ground-state electronic configuration of [Kr]$4d^{10}5s^0$, and Ag-4*d* orbitals fully occupied by electrons are located in energy close to Cl-3p orbitals. Therefore, Ag-4*d* and Cl-3*p* orbitals look being admixed with each other in bonding and anti-bonding manners, which results in the more complicated and broader profile of the valence band in AgCl than that in NaCl. Meanwhile, originally unoccupied Ag-5*s* and 5*p* orbitals have minor contributions to the valence band, which is related to covalency of Ag-Cl bonds. The band gap of less than 2 eV is also smaller than that of NaCl.

3.5 Electronic structures during the {110}<1$\bar{1}$0> slip

The {110}<1$\bar{1}$0> slip system is known to work as the primary slip system in both NaCl and AgCl. However, the Peierls stress and the GSF energy for AgCl are much lower than those of NaCl (see Figs. 2 and 3, and Table 1). In order to investigate a physical origin on the difference, electronic and atomic structures around the {110} plane are analyzed.

Figure 6 (a) shows local densities of states (LDOS) from ions in two atomic layers across the {110} slip plane. Figure 6(b) and 6(c) show densities of states (DOS) and –pCOHPs profiles from ions in the two atomic layers at $u/|\vec{b}|$ = 0.5, respectively. In the case of NaCl, the valence-band profile shows variations with increasing $u/|\vec{b}|$. In particular, it seems that the lower-energy peak in the valence band tends to become broader with rising $u/|\vec{b}|$. This may indicate changes in interactions between Na and Cl across the slip plane during the deformation, because the lower-energy peak arises from the bonding interaction between Na 3*sp* and Cl 3*p*. The valence band profile of AgCl also shows the similar variation against the slip deformation with the NaCl case. In particular, the peaks at around –4 eV tend to become broader with increasing slip deformation. This may also be related to changes in chemical bonding states across the slip plane in AgCl.

In order to understand electronic-structure changes during the slip deformation in more detail, the detailed COHP analyses of ionic pairs across the slip plane were conducted at every $u/|\vec{b}|$. Figure 7(a) illustrates the atomic arrangement across the {110} slip plane, viewed parallel to the slip plane. There are two types of cation-anion pairs, A and B, where the ions in the type-A pair comes close to each other during the slip, while those in the type-B go away from each other. Figure 7(b) shows interionic distances of the type-A pairs as a function of displacement $u/|\vec{b}|$. In this figure, the distances without structural relaxation (rigidly translated) and with structural relaxation are displayed. It can be seen that the interionic distances with relaxation tend to become larger than those without relaxation. This can be simply understood from electronic repulsion between ions across the slip plane. When the slip deformation proceeds from $u/|\vec{b}|$ = 0.0 and the half crystal is rigidly translated, the interionic distance in the type-A

pair becomes smaller, which simultaneously brings about overlap of outermost electrons of the two ions. Therefore, the interionic distance becomes larger, as compared with those without relaxation, so as to decrease energy penalties due to such electronic repulsion of the ions.

A difference in the interionic distance against $u/|\vec{b}|$ can also be found between NaCl and AgCl. Since the lattice parameter of AgCl is slightly smaller than that of NaCl, the interionic distance without relaxation in AgCl shows slightly smaller values than those in NaCl. However, such a difference between AgCl and NaCl tends to be more enhanced by relaxation.

Figure 8(a) shows the –IpCOHP values for ionic pairs across the slip plane as a function of $u/|\vec{b}|$. Since the interionic distance of the type-B pair increases with rising $u/|\vec{b}|$, it is natural that the –IpCOHP value decreases and becomes close to zero at around $u/|\vec{b}| = 0.5$. In contrast, the type-A pair shows larger –IpCOHP value with increasing $u/|\vec{b}|$. In particular, the –IpCOHP value for type-A in AgCl is much larger than that in NaCl. The sum of the –IpCOHP values for the type-A and -B pairs at each $u/|\vec{b}|$ indicates total orbital interactions between ions across the slip plane, and they tend to decrease with increasing $u/|\vec{b}|$. However, the total –IpCOHP for AgCl does not decrease so much as that for NaCl, because of the larger –IpCOHP of the type-A pair in AgCl.

Figure 8(b) displays atomic-orbital resolved –IpCOHP values of the type-A pair in NaCl and AgCl against $u/|\vec{b}|$. It can be seen that –IpCOHP values between cation-*sp* and Cl-3*p* orbitals are positive. Therefore, the increase in –IpCOHP during slip deformation is ascribed to bonding interactions between cation-*sp* and Cl-3*p* orbitals. Especially, Ag-5*s* and Cl-3*p* bonding interactions are much larger, and tend to increase more with increasing $u/|\vec{b}|$, as compared with the other ones. Since such Ag-5*s* and Cl-3*p* interactions give rise to covalent interactions between Ag and Cl, more stronger covalent bonds are formed during the slip deformation in AgCl, which contributes to the smaller GSF energies of $\{110\}\langle 1\bar{1}0\rangle$ in AgCl. It is noted that the stronger bonding interactions between Ag-5*s* and Cl-3*p* orbitals than those between Na-3*s* and Cl-3*p* orbitals are basically due to the smaller band gap of AgCl (see Fig. 5). Ag-5*sp* orbitals forming the conduction band are located in energy closer to Cl-3*p* orbitals, as compared to Na-3*sp* orbitals, which tends to make the bonding interaction stronger.

3.6 Electronic structures during the {111}<1$\bar{1}$0> slip

As described before, the GSF energies and Peierls stresses show that the {111}<1$\bar{1}$0> slip system has a potential to be activated in AgCl whereas that is not an easy slip system in NaCl as reported before [1-3, 22]. In order to discuss such a difference in the {111}<1$\bar{1}$0> slip system between NaCl and AgCl, the similar structural and COHP analyses were carried out.

Figure 9(a) shows LDOS profiles from ions in two atomic layers across the {111} slip plane in NaCl and AgCl at different $u/|\vec{b}|$. Figure 9(b) and 9(c) show DOS and –pCOHPs profiles from ions in the two atomic layers at $u/|\vec{b}| = 0.5$, respectively. The overall trend in the valence band structure changes is similar to the cases in Fig. 6. The valence band width tends to increase with increasing $u/|\vec{b}|$, and some prominent peaks in the valence bands become broader with rising $u/|\vec{b}|$.

Figure 10(a) and 10(b) show the schematic illustrations of atomic arrangements of {111} viewed parallel and normal to the slip plane, respectively. Here the slip deformation can be characterized by four kinds of ionic pairs (from 'A' to 'D') across the slip plane. Figure 10 (c) also shows interionic distances of the type-A pair with and without relaxation as a function of $u/|\vec{b}|$, where the ions in the type-A pair come closest to each other during the slip. It can be seen that the relaxed distances are definitely longer than those without relaxation. In addition, the relaxed distance in AgCl is shorter than that in NaCl. This behavior of the interionic distances is almost the same with that in the {110}<1$\bar{1}$0> slip system (Fig. 7(b)), and this can be thus understood by electronic repulsion between ions across the slip plane during slip deformation.

Figure 11(a) shows the –IpCOHPs for four ionic pairs across the {111} slip plane as a function of $u/|\vec{b}|$. It can be seen that the –IpCOHPs of the type-C and -D pairs decrease with rising $u/|\vec{b}|$ while that of the type-A pair tends to increase. However, the type-A pair in AgCl shows much larger –IpCOHP values that in NaCl. As a result, the total –IpCOHP in AgCl across the slip plane does not exhibit significant decrease against $u/|\vec{b}|$, as compared with that in NaCl. As stated in Fig. 8, the stronger covalent character of bonding in AgCl is due to the bonding overlap between Ag-5*s* and Cl-3*p* orbitals, as also found in Fig. 11(b). The larger covalent

interactions of Ag-Cl makes the {111}<1$\bar{1}$0> slip system more feasible in AgCl.

3.7 Electronic structures during the {111}<2$\bar{1}\bar{1}$> partial slip

The calculated GSF energies show that the {111}<2$\bar{1}\bar{1}$> partial slip is possible in NaCl and AgCl. It is essential to discuss characters in the {111}<2$\bar{1}\bar{1}$> partial slip for understanding slip deformation on {111} in NaCl and AgCl. Therefore, the similar structural and COHP analyses were carried out. Here note that only the range from $u/|\vec{b}|$ = 0 to 1/3 is discussed in this section, since partial slip joins perfect structure via the displacement at $u/|\vec{b}|$ = 1/3 without undergoing that at $u/|\vec{b}|$ = 2/3, as described in the section 3.3.

Figure 12(a) shows LDOS profiles from ions in two atomic layers across the {111} slip plane in NaCl and AgCl at different $u/|\vec{b}|$. Figure 12(b) and 12(c) show DOS and –pCOHPs profiles from ions in the two atomic layers at $u/|\vec{b}|$ = 0.5, respectively. The overall trend in the valence band structure changes is quite similar to the cases in Fig. 6. The valence band width tends to increase with increasing $u/|\vec{b}|$, and some prominent peaks in the valence bands become broader with rising $u/|\vec{b}|$.

Figure 13(a) shows the schematic illustrations of atomic arrangements of {111} viewed normal to the slip plane, respectively. This slip deformation can be characterized by three kinds of ionic pairs (from 'A' to 'C') across the slip plane. Figure 13(b) also shows interionic distances of the type-A pair with and without relaxation as a function of $u/|\vec{b}|$. Here the ions in the two type-A pairs come closest to each other during the slip. Note that type-C pair is equivalent to a type-A pair at $u/|\vec{b}|$ = 0 and that type-B pair is equivalent to a type-A pair at $u/|\vec{b}|$ = 1/3. It is characteristic in {111}<2$\bar{1}\bar{1}$> partial slip that the interionic distances of type-A initially decrease, and again increase after the minimum. It can be also seen that the relaxed distances are definitely longer than those without relaxation. In addition, the relaxed distance in AgCl is shorter than that in NaCl. This behavior can be understood by electronic repulsion between ions across the slip plane during slip deformation.

Figure 14(a) shows the –IpCOHPs for the type-A pair and the sum of type-B and -C pairs across the {111} slip plane as a function of $u/|\vec{b}|$. It can be seen that the –IpCOHPs of the sum

of type-B and -C pairs decrease once with rising $u/|\vec{b}|$ and then increase while that of the type-A pair varies in the opposite way. In addition, the total –IpCOHP in NaCl does not exhibit significant decrease against $u/|\vec{b}|$ as compared to those in the {111}<1$\bar{1}$0> slip (Fig. 11(a)). These behaviors can be explained by the increase and decrease of interionic distances shown in Fig. 13(b). Atomic-orbital resolved COHP analyses in Fig. 14(b) say that the covalent character of bonding in AgCl is ascribed to the bonding overlap between Ag-5*s* and Cl-3*p* orbitals. This trend is similar to the cases in the other slip systems.

3.8 Electronic structures during the {001}<110> slip

The calculated GSF energies in Figs. 2 and 3 predict that the {001}<110> slip system works in AgCl but does not in NaCl. It is interesting that the slip deformation on the {001} plane is available in AgCl, although the {001} plane is typically the cleavage plane of the rock-salt structured ionic crystals.

Figure 15(a) shows LDOS profiles from ions in two atomic layers across the {001} slip plane in NaCl and AgCl. Figure 15(b) and 15(c) show PDOS and –pCOHPs profiles from ions in the two atomic layers at $u/|\vec{b}| = 0.5$, respectively. In the case of NaCl, since the slab models were separated into two halves, only LDOSs at $u/|\vec{b}|$ of up to 0.3 are displayed. As stated above in the other slip systems, the valence band widths become larger with increasing $u/|\vec{b}|$. In particular, it seems that the shape of the valence band of AgCl changes more severely than those in Figs. 6, 9 and 12 for the other slip systems. The band gap of AgCl also tends to decrease more with rising $u/|\vec{b}|$, which is more evident than those in the other slip systems. In addition, bonding character between Ag ions appears to be more prominent while the bonding character between Ag and Cl ions is weakened, as can be seen from the profile at $u/|\vec{b}| = 0.5$ in Fig. 15(c).

Figure 16(a) and 16(b) display illustrations of atomic arrangements around the slip plane. In this case, there are three types of ionic pairs across the slip plane, where cation-cation or anion-anion pairs are denoted by the type-A and a cation-anion pair is described by the type-B. Figure 16(c) shows interionic distances of type-A pairs as a function of $u/|\vec{b}|$. When the slip deformation proceeds from $u/|\vec{b}| = 0.0$, like ions in the type-A pairs come close to each other,

and thus the interionic distances tend to decrease with rising $u/|\vec{b}|$. That can be imagined from the plot for the case without relaxation. In the case of NaCl, the interionic distances of Na-Na and Cl-Cl abruptly increase at $u/|\vec{b}| = 0.3$, which corresponds to cleavage on the {001} plane.

In contrast, the interionic distances of Ag-Ag and Cl-Cl decrease monotonically up to $u/|\vec{b}| = 0.5$. It is surprising here, however, that the Ag-Ag distance tends to decrease more, even compared with that without relaxation. Since Ag-Ag pairs have the same positive ionic charges, it is natural to think that the interionic distance may become larger due to electrostatic repulsion than that without relaxation. Contrary to this expectation, Ag-Ag pairs across the slip plane of {001} favors more close proximity during the slip deformation.

In order to investigate the transition of chemical bonding states across the slip plane, the detailed COHP analyses were performed. As can be seen in Fig. 17(a), the –IpCOHP values for the type-B cation-anion pair tend to decrease with increasing $u/|\vec{b}|$. This can be easily imagined from the fact that the interionic distance of the type-B pair increases with rising $u/|\vec{b}|$ (see Fig. 16). It can also be seen that type-A Cl-Cl pairs in both NaCl and AgCl exhibit negative –IpCOHP values. This is because that Cl ions with a negative ionic charge of –1 have the fully occupied electronic shell of [Ne]$3s^2 3p^6$ and their overlap in a bonding manner are prohibited by the Pauli's exclusion principle. As compared to the ionic pair of Cl-Cl, it is evident that the Ag-Ag pair exhibits the quite large positive –IpCOHP values with increasing $u/|\vec{b}|$. It can be said, therefore, that formation of covalent Ag-Ag bond across the slip plane takes place. Such covalent bonds between cations cannot be found in NaCl. Atomic-orbital resolved COHP analyses in Fig. 17(b) say that the covalent Ag-Ag bonds across the slip plane is ascribed to bonding overlaps between Ag-5*sp* and Ag-4*d* orbitals.

Such bonding interactions between Ag ions across the slip plane can be explained from the basic electronic structure of AgCl. As stated in Fig. 5, NaCl has the large band gap, which indicates that energies of outermost Na-3*sp* and Cl-3*p* orbitals are quite different from each other and thus the bonding overlap between the atomic orbitals is quite small. This is the fact to prove that NaCl is a typical ionic crystal. In contrast, AgCl has the smaller band gap, and also the electron occupied 4*d* orbitals take part in the valence band. During the slip motion, Ag

ions often come close to each other, and outermost Ag-5*sp* orbitals have bonding interactions with Ag-4*d* orbitals across the slip plane. This can be realized because Ag-4*d* orbitals have an energy close to Cl-3*p* orbitals in the valence band. In this point, since Na-2*p* orbitals are located in energy far below Cl-3*p* orbitals, the outermost Na-3*sp* orbitals cannot interact with atomic orbitals at the Na core across the slip plane. Although Cl-Cl pairs simultaneously have repulsive interactions during the slip, the bonding interaction of Ag-Ag is much larger than the anti-bonding one of Cl-Cl. This can also be confirmed in Fig. 17(a), where the absolute value of –IpCOHP for Ag-Ag is much larger than that of Cl-Cl.

As a final note, it is necessary to mention that the slip system of {001}<100> would not be available even in AgCl as well as in NaCl (see Figs. 2 and 3). Even on the same {001} plane, the mechanism of Ag-Ag formation depends on the slip direction. The reason for this issue can be discussed by atomic arrangements during the two different slip directions (see Fig. 18). In the case of the {001}<100> system, all ions are located atop like ions below the slip plane at the displacement of $u/|\vec{b}| = 0.5$. It is expected that all ions are subjected to strong electrostatic repulsion across the slip plane, which makes cleavage by this slip motion easily occur. In contrast, all ions are located at interstitial regions of ions below the slip plane at $u/|\vec{b}| = 0.5$ in the {001}<110> system. In this case, all ions are coordinated by two like and unlike ions across the slip plane. In fact, as can be seen in Fig. 17(b), the –IpCOHP value for the type-B Ag-Cl pair is not negligible even at $u/|\vec{b}| = 0.5$, although the Cl-Cl interaction is anti-bonding. Moreover, covalent bonds are formed between Ag ions across the slip plane. These covalent interactions of Ag-Ag as well as Ag-Cl across the slip plane may compensate energy costs due to like ions approaching during the slip. This can be realized along the slip direction of <110>.

4. Conclusions

First-principles calculations were performed to investigate the difference in available slip systems between NaCl and AgCl with the same rock salt structure. The present GSF energy calculations clearly demonstrated that only the {110}<1$\bar{1}$0> slip system is favorably activated in NaCl whereas AgCl shows three kinds of possible slip systems along the <1$\bar{1}$0> direction on

the {001}, {110}, and {111} plane, which is in excellent agreement with experiment. It was also found that the GSF profile for the primary {110}<1$\bar{1}$0> slip system in AgCl exhibits a local minimum against shear displacement, which indicates a possibility of dissociation of the perfect dislocation into Shockley partial dislocations. This should also be related to more ductility of AgCl than NaCl.

In order to explain the difference between NaCl and AgCl, detailed valence band structures during slip deformation were investigated. In particular, quantitative changes in interactions between atomic orbitals across the slip planes were analyzed by the COHP method. It was found that the more covalent character of bonding of Ag-Cl than Na-Cl tends to make the slip deformation energetically favorable. This can be attributed to the difference in fundamental electronic structures between NaCl and AgCl. It was also surprising to find out that strong Ag-Ag covalent bonds across the slip plane are formed in the {001}<110> slip system in AgCl. Such specific bonding of like ions makes the multiple slip systems available without cleavage in AgCl.

Acknowledgements

The authors gratefully acknowledge the financial support by a Grant-in-Aid for Scientific Research on Innovative Areas "Nano Informatics" (grant numbers 25106002) from Japan Society for the Promotion of Science (JSPS). This study was partly supported by JSPS KAKENHI Grant Numbers 25630279, 26630311, 15K14122, 15H04145, 15K14123 and 16K14414.

References

1. J.P. Hirth and J. Lothe, *Theory of dislocations,* 2nd ed., Willey, New York, 1982.
2. T. Suzuki and S. Takeuchi, *Deformation of Crystals Controlled by the Peierls Mechanism of the Smooth Kink Regime*, Crystal Lattice Defects and Dislocation Dynamics, R. A. Vardanian, eds., Nova Science Pub., New York, 2001, pp. 1–70.
3. C.M. Van Der Walt and M.J. Sole, *On the plastic behaviour of crystals with the NaCl-structure*, Acta Metall. 15 (1967), pp. 459–462.
4. J.F. Nye, *Plastic Deformation of Silver Chloride. I. Internal Stresses and the Glide Mechanism*, Proc. Royal Soc. A 198 (1949), pp. 190–204.
5. F. Vávra, *Etch pits in AgCl crystals*, Czech. J. Phys. B 19 (1969), pp. 776–782.
6. F. Vávra and Z. Ševčík, *Formation of wavy slip bands in AgCl crystals at low temperatures*, Czech. J. Phys. B 36 (1986), pp. 509–513.
7. V. Vitek, *Intrinsic stacking faults in body-centred cubic crystals*, Phil. Mag. 18 (1968), pp. 773–786.
8. N. De Leon, X. Yu, H. Yu, C.R. Weinberger, and G. B. Thompson, Bonding effects on the slip differences in the B1 monocarbides, Phys. Rev. Lett., 114 (2015) 165502.
9. R. Peierls, *The size of a dislocation*, Proc. Phys. Soc. 52 (1940), pp. 34–37.
10. F.R.N. Nabarro, *Dislocations in a simple cubic lattice*, Proc. Phys. Soc. 59 (1947), pp. 256–272.
11. R. Dronskowski and P.E. Bloechl, *Crystal orbital Hamilton populations (COHP): energy-resolved visualization of chemical bonding in solids based on density-functional calculations*, J. Phys. Chem. 97 (1993), pp. 8617–8624.
12. G. Kresse and J. Furthmüller, *Efficient iterative schemes for ab initio total-energy calculations using a plane-wave basis set*, Phys. Rev. B 54 (1996), 11169.
13. P.E. Blöchl, *Projector augmented-wave method*, Phys. Rev. B 50 (1994), 17953.
14. J.P. Perdew, K. Burke, and M. Ernzerhof, *Generalized gradient approximation made simple*, Phys. Rev. Lett. 77 (1996), 3865.
15. V.L. Deringer, A.L. Tchougréeff, and R. Dronskowski, *Crystal Orbital Hamilton*

Population (COHP) Analysis As Projected from Plane-Wave Basis Sets, J. Phys. Chem. A 115 (2011), pp. 5461–5466.

16. S. Maintz, V.L. Deringer, A.L. Tchougréeff, and R. Dronskowski, *Analytic projection from plane-wave and PAW wavefunctions and application to chemical-bonding analysis in solids*, J. Comp. Chem. 34 (2013), pp. 2557–2567.
17. M. Bruno, D. Aquilano, L. Pastero, and M. Prencipe, *Structures and Surface Energies of (100) and Octopolar (111) Faces of Halite (NaCl): an Ab initio Quantum-Mechanical and Thermodynamical Study*, Crys. Growth & Design 8 (2008), pp. 2163–2170.
18. M. Bruno, D. Aquilano, and M. Prencipe, *Quantum-Mechanical and Thermodynamical Study on the (110) and Reconstructed (111) Faces of NaCl Crystals*, Crys. Growth & Design 9 (2009), pp. 1912–1916.
19. L. Liu, X.Z. Wua, R. Wang, H.F. Feng, and S. Wu, *On the generalized stacking energy, core structure and Peierls stress of the dislocations in alkali halide*, Euro. Phys. J. B. 85 (2012), 58.
20. B. Joós and M. S. Duesbery, *The Peierls Stress of Dislocations: An Analytic Formula*, Phys. Rev. Lett. 78 (1997), pp. 266–269.
21. Y. Li, L. Zhang, T. Cui, Y. Ma, G. Zou, and D.D. Klug, *Phonon instabilities in rocksalt AgCl and AgBr under pressure studied within density functional theory*, Phys. Rev. B 74 (2006), 054102.
22. Y. Kamimura, K. Edagawa, and S. Takeuchi, *Experimental evaluation of the Peierls stresses in a variety of crystals and their relation to the crystal structure*, Acta Mater. 61 (2013), 294–309.

Figure Captions

Figure 1

Schematic illustrations of the slip planes and directions considered in the present study. (a) {001}<100> and {001}<110>, (b) {110}<001> and {110}<1$\bar{1}$0>, (c) {111}<1$\bar{1}$0> and {111}<2$\bar{1}\bar{1}$>. The *p* indicated with blue solid arrows correspond to the normal vectors of individual slip planes of {001}, {110} and {111}.

Figure 2

The calculated GSF energies as a function of displacement $u/|\vec{b}|$ in NaCl. Here $u/|\vec{b}|$ are indicated by 'u/b' in figures. (a) and (b) correspond to the slip directions of <100> and <110>, respectively.

Figure 3

The calculated GSF energies as a function of displacement $u/|\vec{b}|$ in AgCl. (a) and (b) correspond to the slip directions of <100> and <110>, respectively.

Figure 4

(a) Atomic arrangement of the {111} plane and the Burgers vectors for a perfect dislocation and those for Shockley partial dislocations. (b) GSF energies for the <1$\bar{1}$0> and <2$\bar{1}\bar{1}$> slips in NaCl as a function of the distance. (c) GSF energies for the <1$\bar{1}$0> and <2$\bar{1}\bar{1}$> slips in AgCl as a function of the distance. Blue broken lines in (b) and (c) correspond to the displacements from "A" to "C" in (a).

Figure 5

Electronic structures in the valence bands of perfect NaCl and AgCl. The energy bands located below 0 eV mean the ones occupied by electrons. (a) Atomic-orbital components in the DOS curves. (b) –pCOHP profiles.

Figure 6

Electronic structures in the two atomic layers across the slip plane in {110}<1$\bar{1}$0> slip of NaCl and AgCl. (a) Local DOS curves. Red arrows in the figure represent positions of the conduction-band bottoms. (b) Atomic-orbital components in the DOS curves at $u/|\vec{b}|$ = 0.5. (c) –pCOHP profiles at $u/|\vec{b}|$ = 0.5.

Figure 7

(a) Schematic illustration of atomic arrangement in the {110}<1$\bar{1}$0> slip system, viewed along the slip plane. Small and large circles in the figure represent positive and negative ions, respectively. In addition, the ions with negative charge on a back atomic layer are drawn using large circles with dashed line. The structural change across the slip plane can be characterized by two ionic pairs named as type-A and type-B. (b) Interionic distances for the type-A pairs in NaCl and AgCl as a function of $u/|\vec{b}|$.

Figure 8

(a) –IpCOHP values of ionic pairs across the slip plane in the {110}<1$\bar{1}$0> system as a function of $u/|\vec{b}|$. (b) Atomic-orbital resolved –IpCOHP values for the type-A pairs.

Figure 9

Electronic structures in the two atomic layers across the slip plane in {111}<1$\bar{1}$0> slip of NaCl and AgCl. (a) Local DOS curves. Red arrows in the figure represent positions of the conduction-band bottoms. (b) Atomic-orbital components in the DOS curves at $u/|\vec{b}|$ = 0.5. (c) –pCOHP profiles at $u/|\vec{b}|$ = 0.5.

Figure 10

Schematic illustrations of atomic arrangements in the {111}<1$\bar{1}$0> slip system, viewed along the slip plane (a) and perpendicular to the slip plane (b). These are drawn in the same manner

with Fig. 7. Interionic distances for the type-A pairs in NaCl and AgCl as a function of $u/|\vec{b}|$ are shown in (c).

Figure 11

(a) –IpCOHP values of ionic pairs across the slip plane in the {111}<1$\bar{1}$0> system as a function of $u/|\vec{b}|$. (b) Atomic-orbital resolved –IpCOHP values for the type-A pairs.

Figure 12

Electronic structures in the two atomic layers across the slip plane in {111}<2$\bar{1}\bar{1}$> partial slip of NaCl and AgCl. (a) Local DOS curves. Red arrows in the figure represent positions of the conduction-band bottoms. (b) Atomic-orbital components in the DOS curves at $u/|\vec{b}| = 1/3$. (c) –pCOHP profiles at $u/|\vec{b}| = 1/3$.

Figure 13

(a) Schematic illustrations of atomic arrangements in the {111}<2$\bar{1}\bar{1}$> partial slip viewed normal to the slip plane. These are drawn in the same manner with Figs. 7 and 10. (b) Interionic distances for the type-A pairs in NaCl and AgCl as a function of $u/|\vec{b}|$.

Figure 14

(a) –IpCOHP values of ionic pairs across the slip plane in the {111}<2$\bar{1}\bar{1}$> partial slip as a function of $u/|\vec{b}|$. (b) Atomic-orbital resolved –IpCOHP values for the type-A pairs.

Figure 15

Electronic structures in the two atomic layers across the slip plane in {001}<110> slip of NaCl and AgCl. (a) Local DOS curves. Red arrows in the figure represent positions of the conduction-band bottoms. (b) Atomic-orbital components in the DOS curves at $u/|\vec{b}| = 0.3$ for NaCl and at $u/|\vec{b}| = 0.5$ for AgCl. (c) –pCOHP profiles at $u/|\vec{b}| = 0.3$ for NaCl and at $u/|\vec{b}| = 0.5$ for AgCl.

Figure 16

Schematic illustrations of atomic arrangements in the {001}<110> slip, viewed along the slip plane. (a) $u/|\vec{b}|$ = 0.0, and (b) $u/|\vec{b}|$ = 0.5 (with relaxation). These are drawn in the same manner with Figs. 7, 10 and 13. Interionic distances for the type-A pairs in NaCl and AgCl as a function of $u/|\vec{b}|$ are shown in (c).

Figure 17

(a) –IpCOHP values of ionic pairs across the slip plane in the {001}<110> slip as a function of $u/|\vec{b}|$. (b) Atomic-orbital resolved –IpCOHP values for the type-A Ag-Ag pair.

Figure 18

Illustrations of atomic configurations viewed normal to the slip plane for the {001}<100> and {001}<110> slip systems. Small and large dotted circles display cations and anions located below the slip plane. Upper figures are those before shear displacement, while lower ones after displacement of $u/|\vec{b}|$ = 0.5.

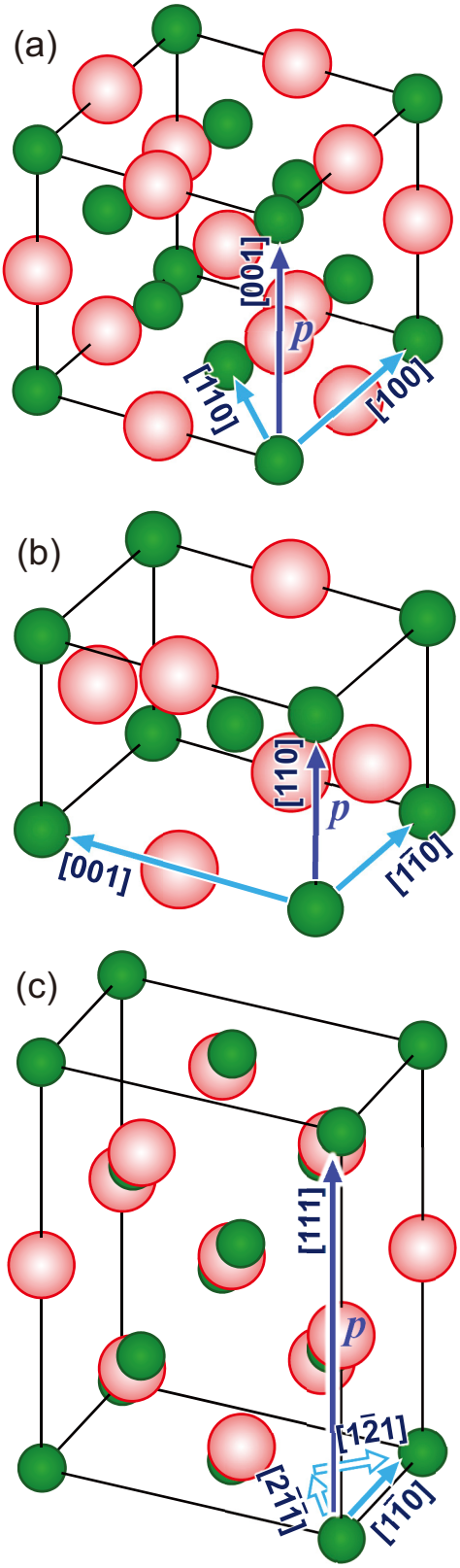

Figure 1. Schematic illustrations of the slip planes and directions considered in the present study. (a) {001}<100> and {001}<110>, (b) {110}<001> and {110}<1$\bar{1}$0>, (c) {111}<1$\bar{1}$0> and {111}<2$\bar{1}\bar{1}$>. The *p* indicated with blue solid arrows correspond to the normal vectors of individual slip planes of {001}, {110} and {111}.

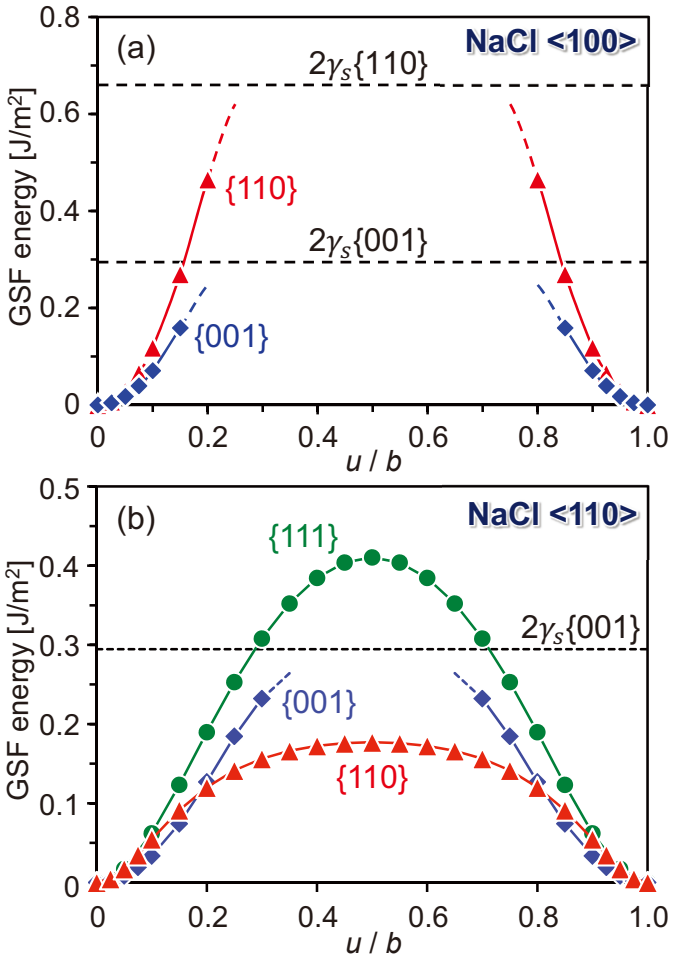

Figure 2. The calculated GSF energies as a function of displacement $u/|\vec{b}|$ in NaCl. Here $u/|\vec{b}|$ are indicated by '*u*/*b*' in figures. (a) and (b) correspond to the slip directions of <100> and <110>, respectively.

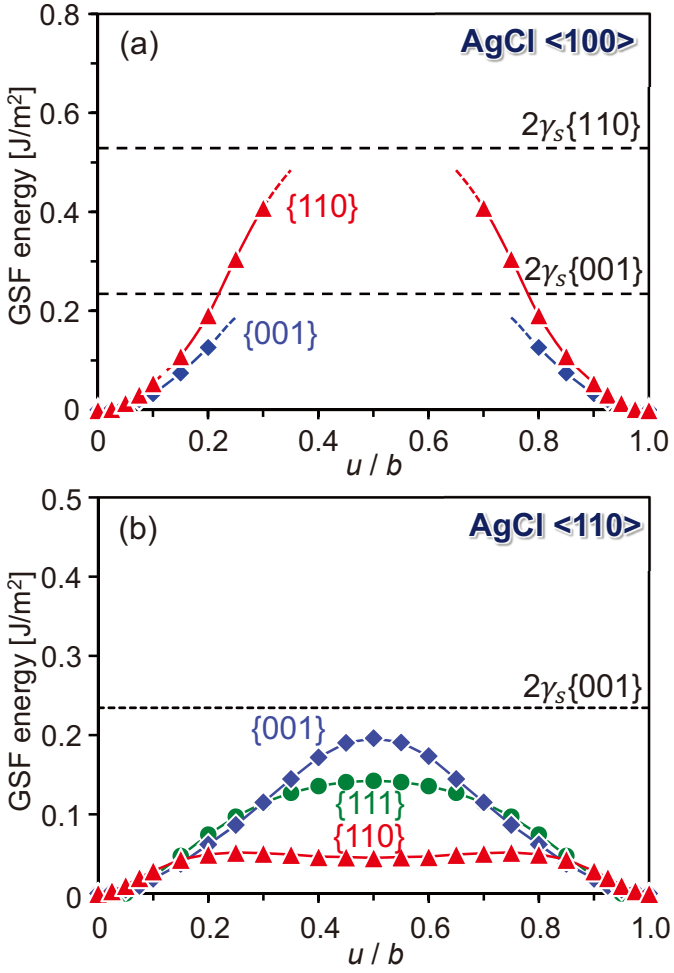

Figure 3. The calculated GSF energies as a function of displacement $u/|\vec{b}|$ in AgCl. (a) and (b) correspond to the slip directions of <100> and <110>, respectively.

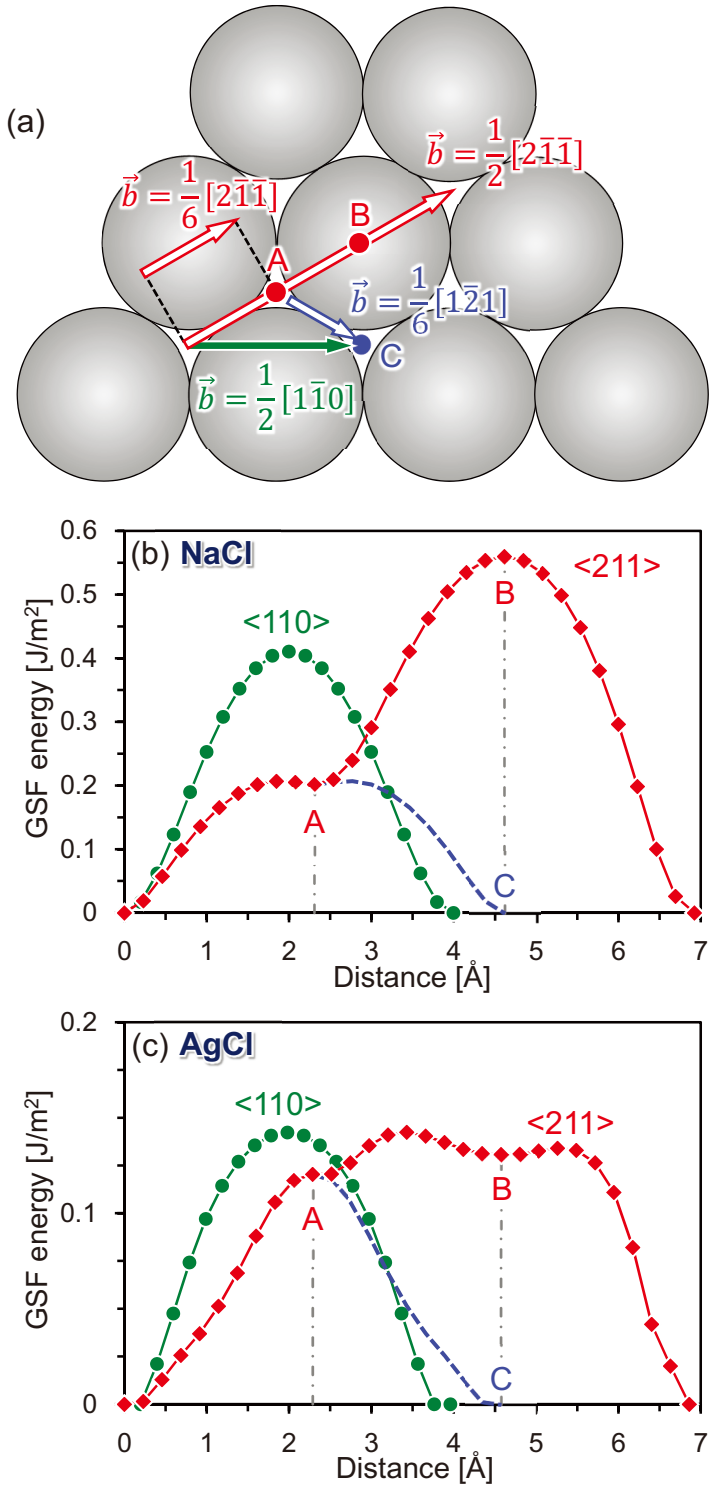

Figure 4. (a) Atomic arrangement of the {111} plane and the Burgers vectors for a perfect dislocation and those for Shockley partial dislocations. (b) GSF energies for the <1$\bar{1}$0> and <2$\bar{1}\bar{1}$> slips in NaCl as a function of the distance. (c) GSF energies for the <1$\bar{1}$0> and <2$\bar{1}\bar{1}$> slips in AgCl as a function of the distance. Blue broken lines in (b) and (c) correspond to the displacements from "A" to "C" in (a)

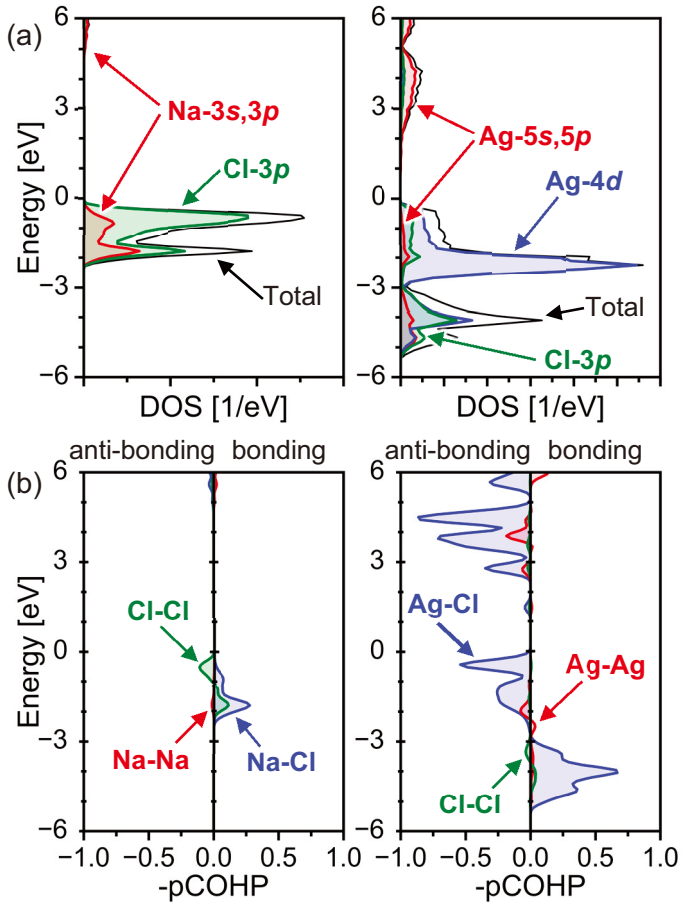

Figure 5. Electronic structures in the valence bands of perfect NaCl and AgCl. The energy bands located below 0 eV mean the ones occupied by electrons. (a) Atomic-orbital components in the DOS curves. (b) –pCOHP profiles.

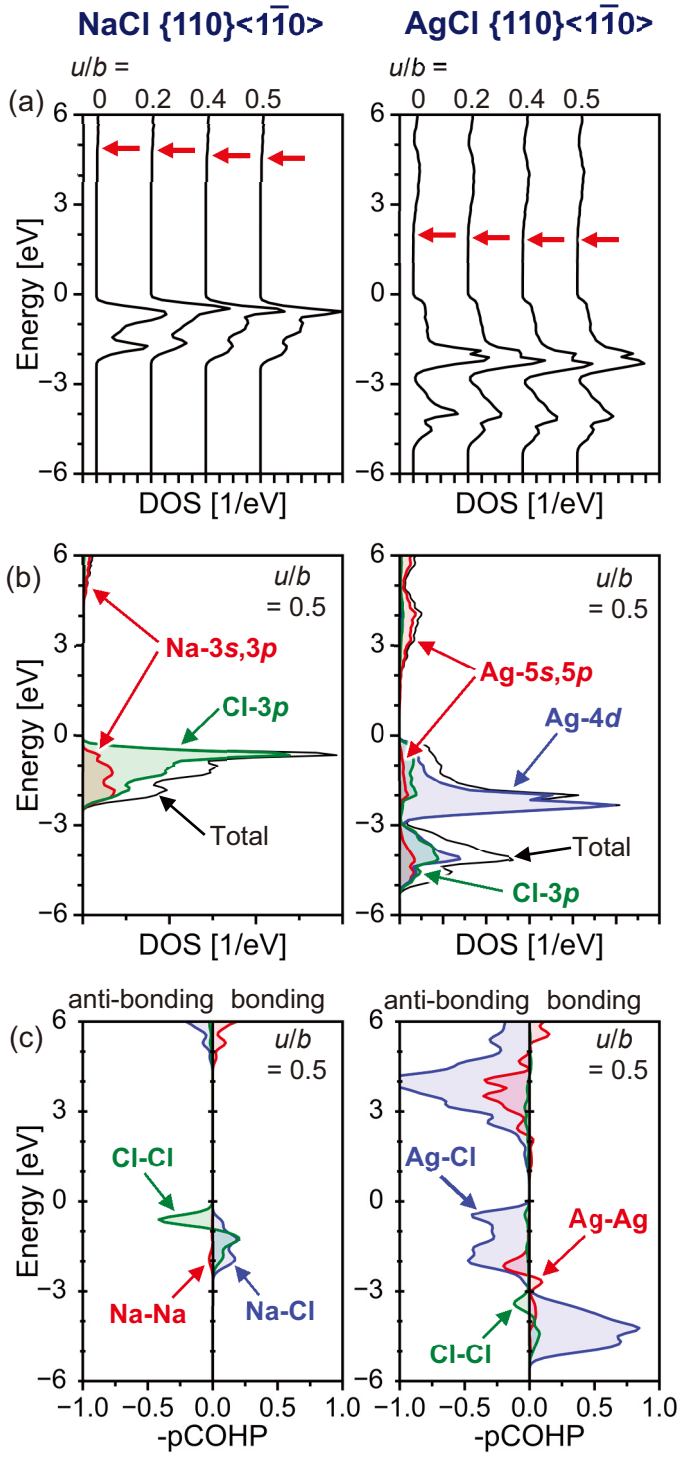

Figure 6. Electronic structures in the two atomic layers across the slip plane in {110}<1$\bar{1}$0> slip of NaCl and AgCl. (a) Local DOS curves. Red arrows in the figure represent positions of the conduction-band bottoms. (b) Atomic-orbital components in the DOS curves at $u/|\vec{b}| = 0.5$. (c) –pCOHP profiles at $u/|\vec{b}| = 0.5$.

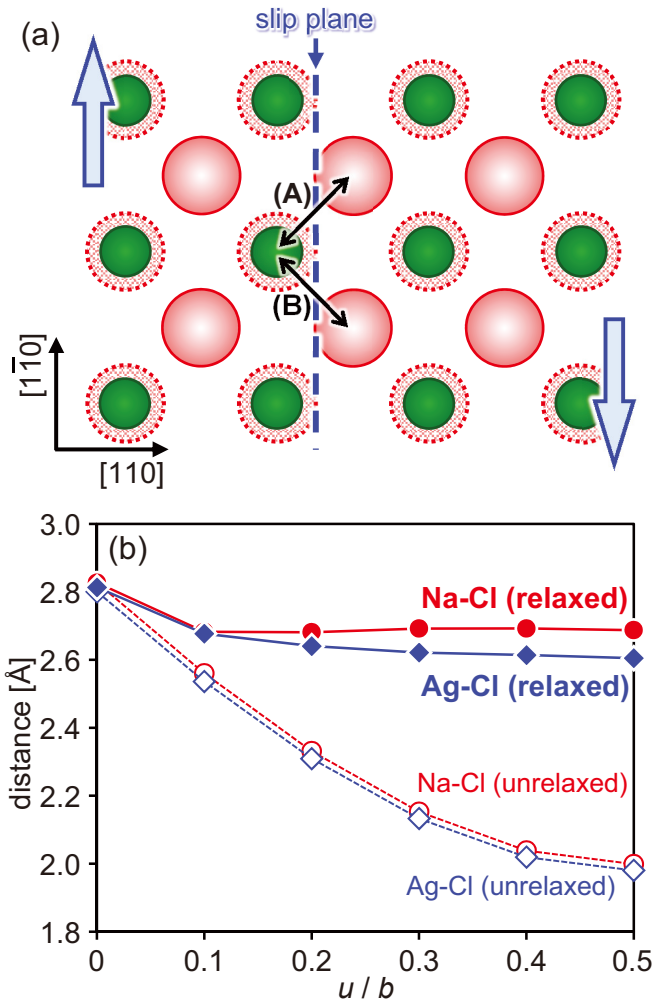

Figure 7. (a) Schematic illustration of atomic arrangement in the {110}<1$\bar{1}$0> slip system, viewed along the slip plane. Small and large circles in the figure represent positive and negative ions, respectively. In addition, the ions with negative charge on a back atomic layer are drawn using large circles with dashed line. The structural change across the slip plane can be characterized by two ionic pairs named as type-A and type-B. (b) Interionic distances for the type-A pairs in NaCl and AgCl as a function of $u/|\vec{b}|$.

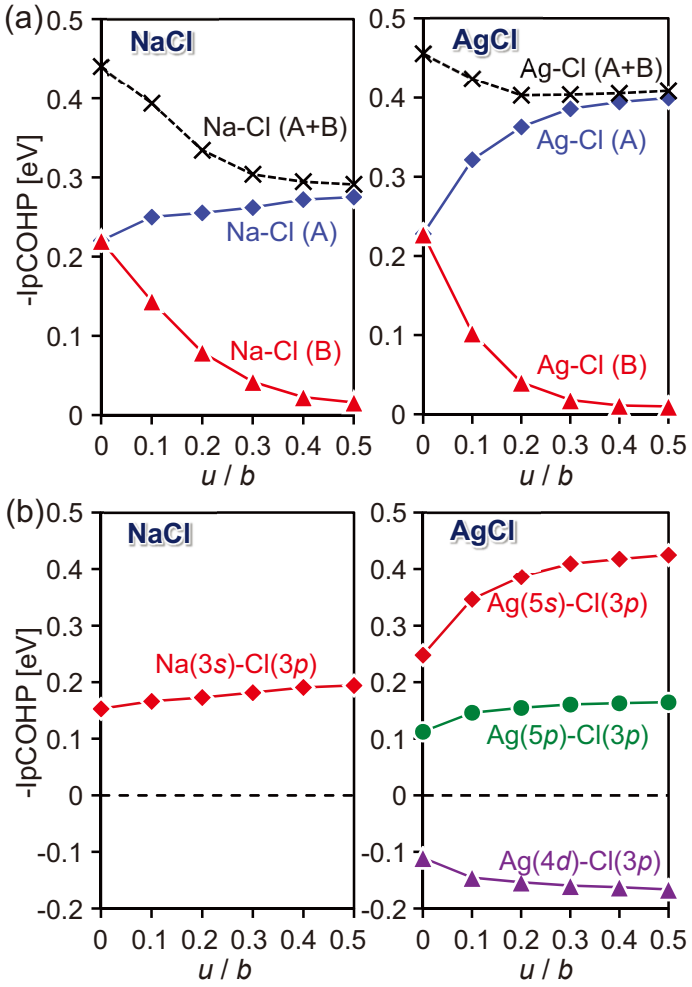

Figure 8 (a) –IpCOHP values of ionic pairs across the slip plane in the {110}<$1\bar{1}0$> system as a function of $u/|\vec{b}|$. (b) Atomic-orbital resolved –IpCOHP values for the type-A pairs.

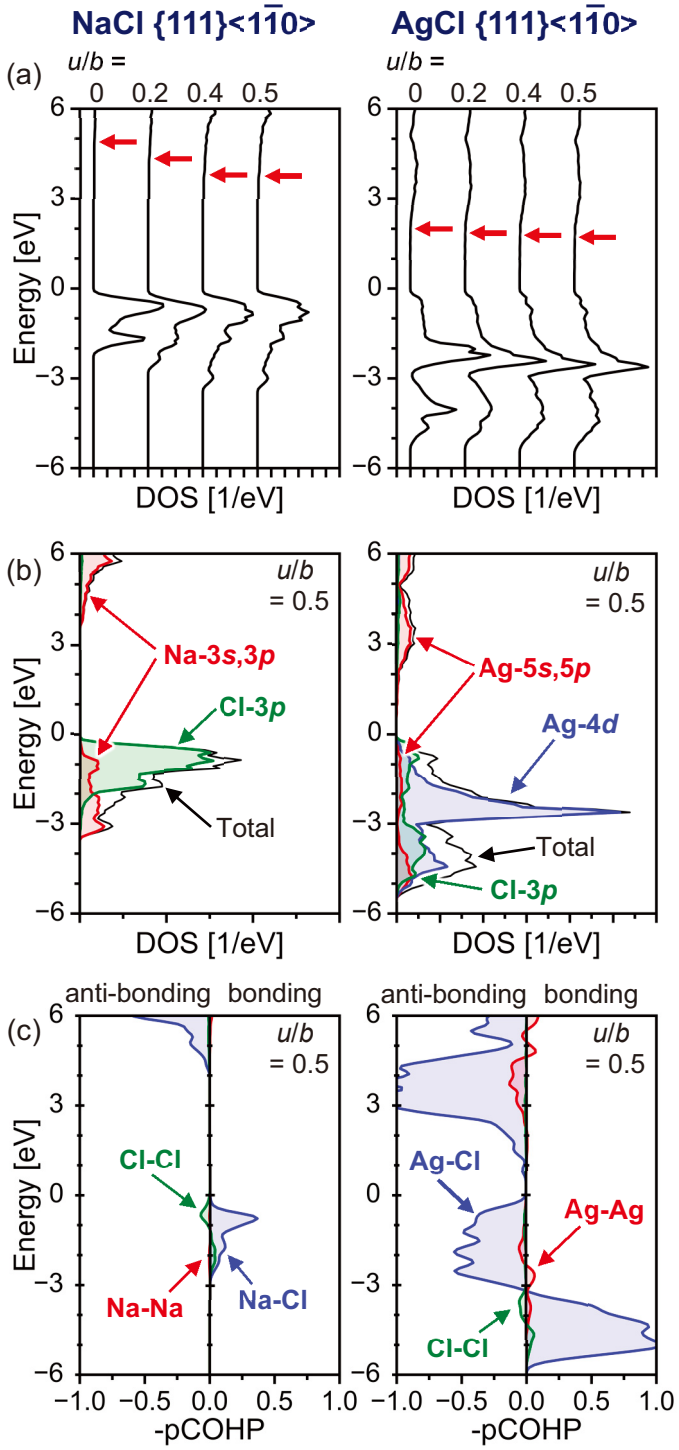

Figure 9. Electronic structures in the two atomic layers across the slip plane in {111}<1$\bar{1}$0> slip of NaCl and AgCl. (a) Local DOS curves. Red arrows in the figure represent positions of the conduction-band bottoms. (b) Atomic-orbital components in the DOS curves at $u/|\vec{b}| = 0.5$. (c) –pCOHP profiles at $u/|\vec{b}| = 0.5$.

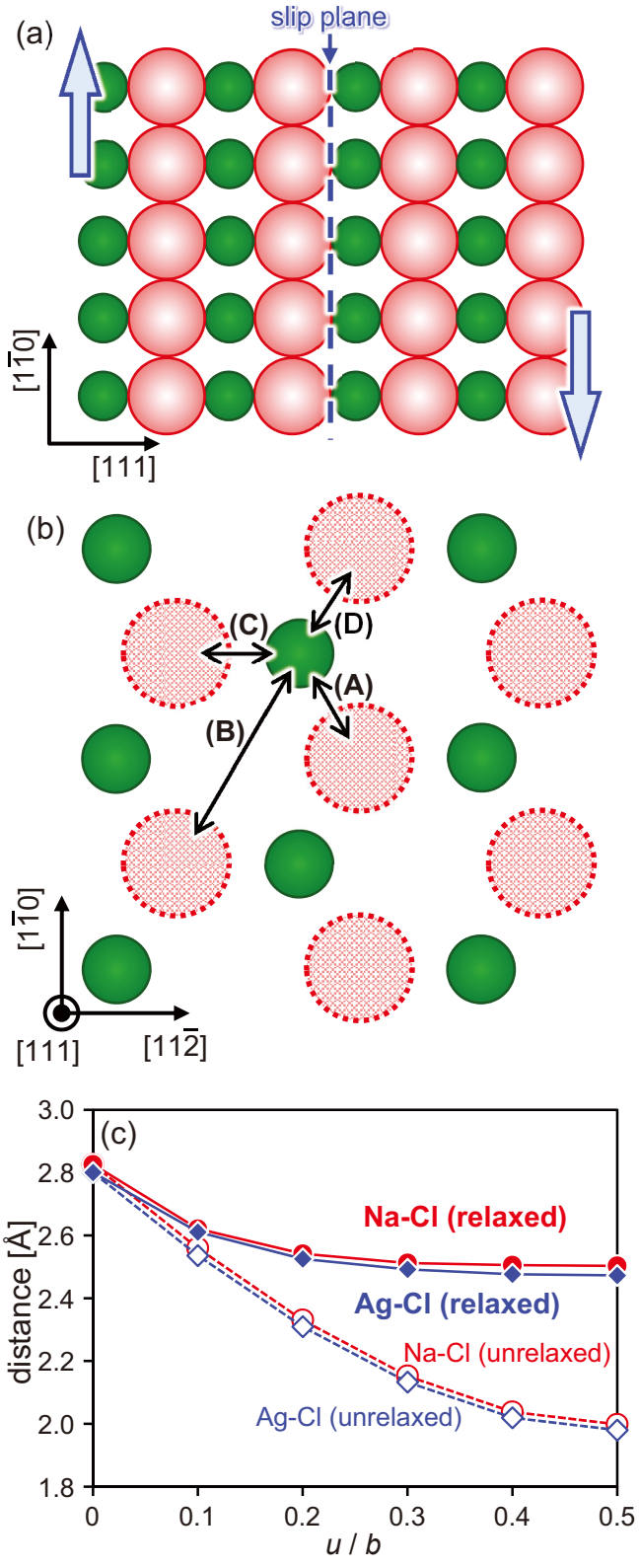

Figure 10. Schematic illustrations of atomic arrangements in the {111}<1$\bar{1}$0> slip system, viewed along the slip plane (a) and perpendicular to the slip plane (b). These are drawn in the same manner with Fig. 7. Interionic distances for the type-A pairs in NaCl and AgCl as a function of $u/|\vec{b}|$ are shown in (c).

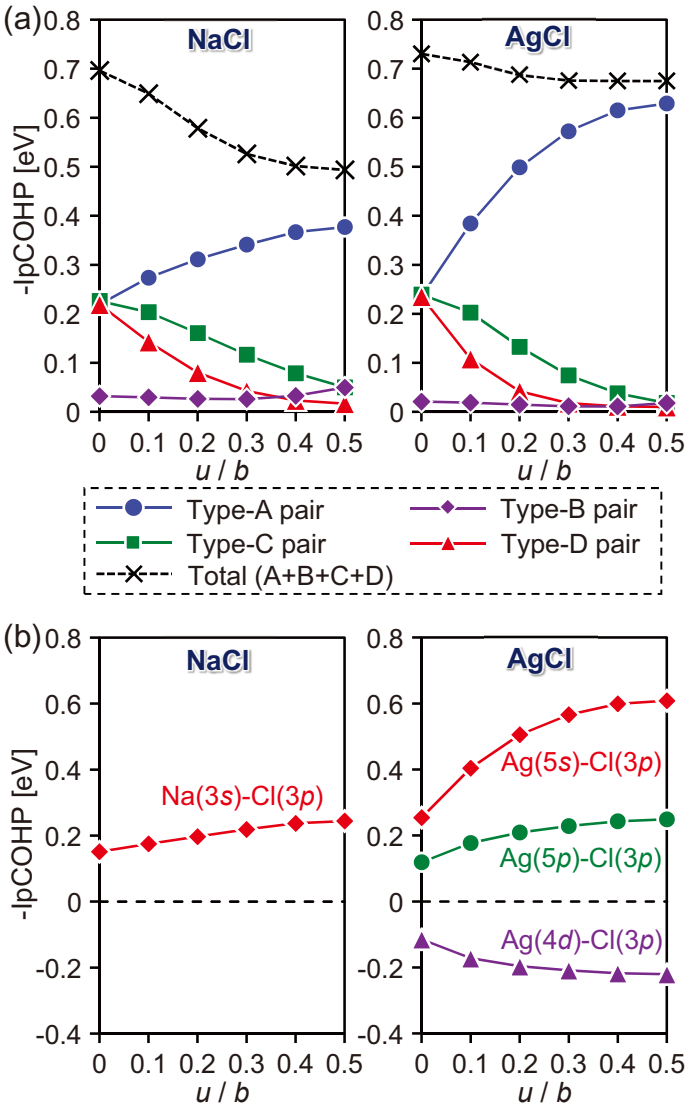

Figure 11. (a) –IpCOHP values of ionic pairs across the slip plane in the {111}<$1\bar{1}0$> system as a function of $u/|\vec{b}|$. (b) Atomic-orbital resolved –IpCOHP values for the type-A pairs.

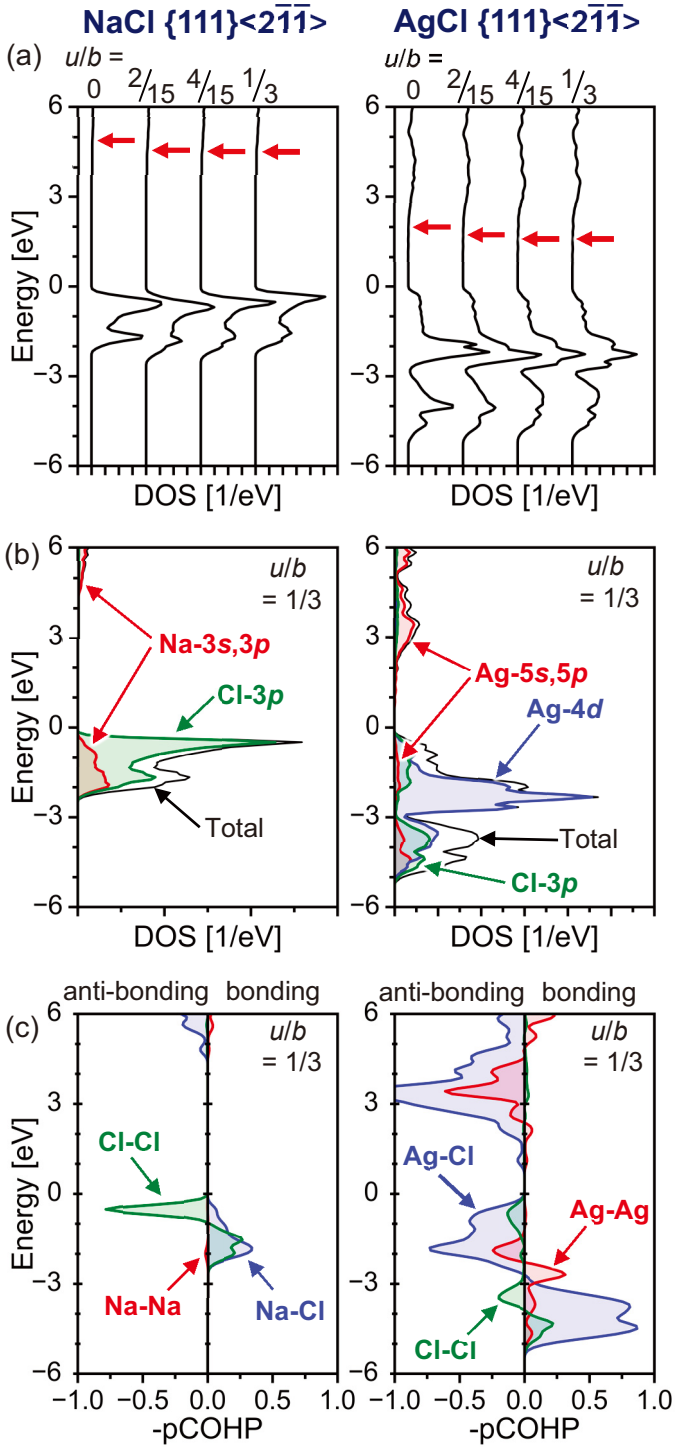

Figure 12. Electronic structures in the two atomic layers across the slip plane in {111}<2$\bar{1}\bar{1}$> partial slip of NaCl and AgCl. (a) Local DOS curves. Red arrows in the figure represent positions of the conduction-band bottoms. (b) Atomic-orbital components in the DOS curves at $u/|\vec{b}|$ = 1/3. (c) –pCOHP profiles at $u/|\vec{b}|$ = 1/3.

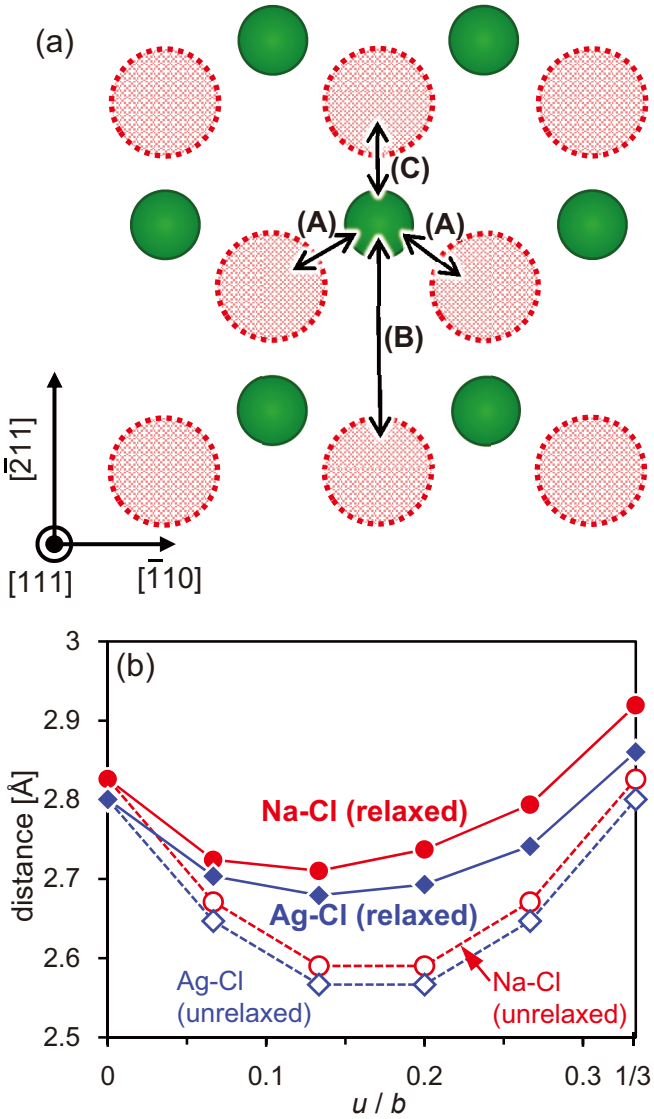

Figure 13. (a) Schematic illustrations of atomic arrangements in the {111}<$2\bar{1}\bar{1}$> partial slip viewed normal to the slip plane. These are drawn in the same manner with Figs. 7 and 10. (b) Interionic distances for the type-A pairs in NaCl and AgCl as a function of $u/|\vec{b}|$.

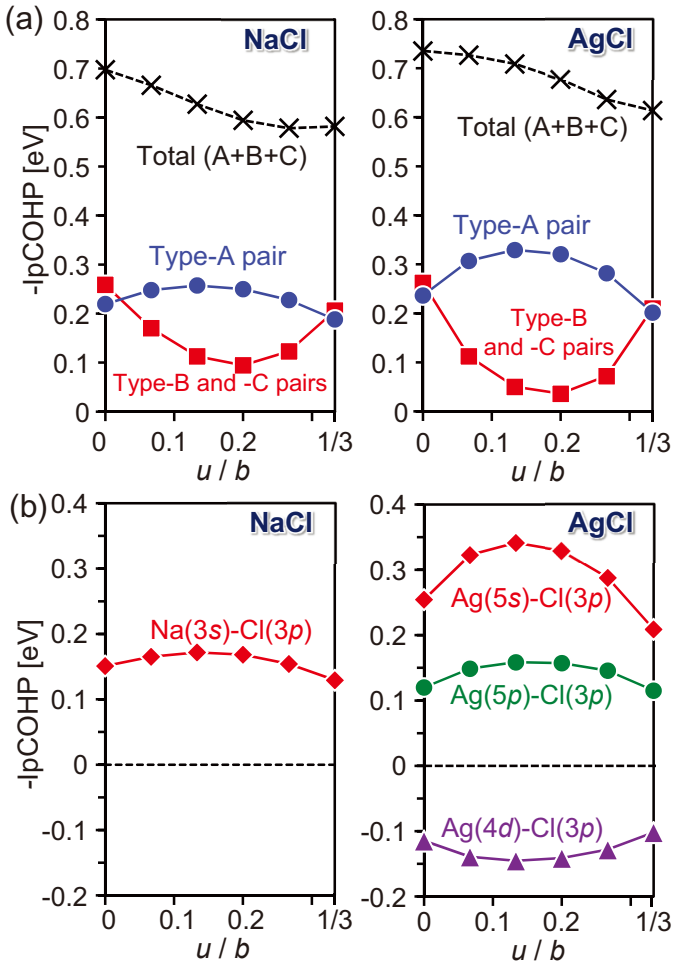

Figure 14. (a) –IpCOHP values of ionic pairs across the slip plane in the {111}<$2\bar{1}\bar{1}$> partial slip as a function of $u/|\vec{b}|$. (b) Atomic-orbital resolved –IpCOHP values for the type-A pairs.

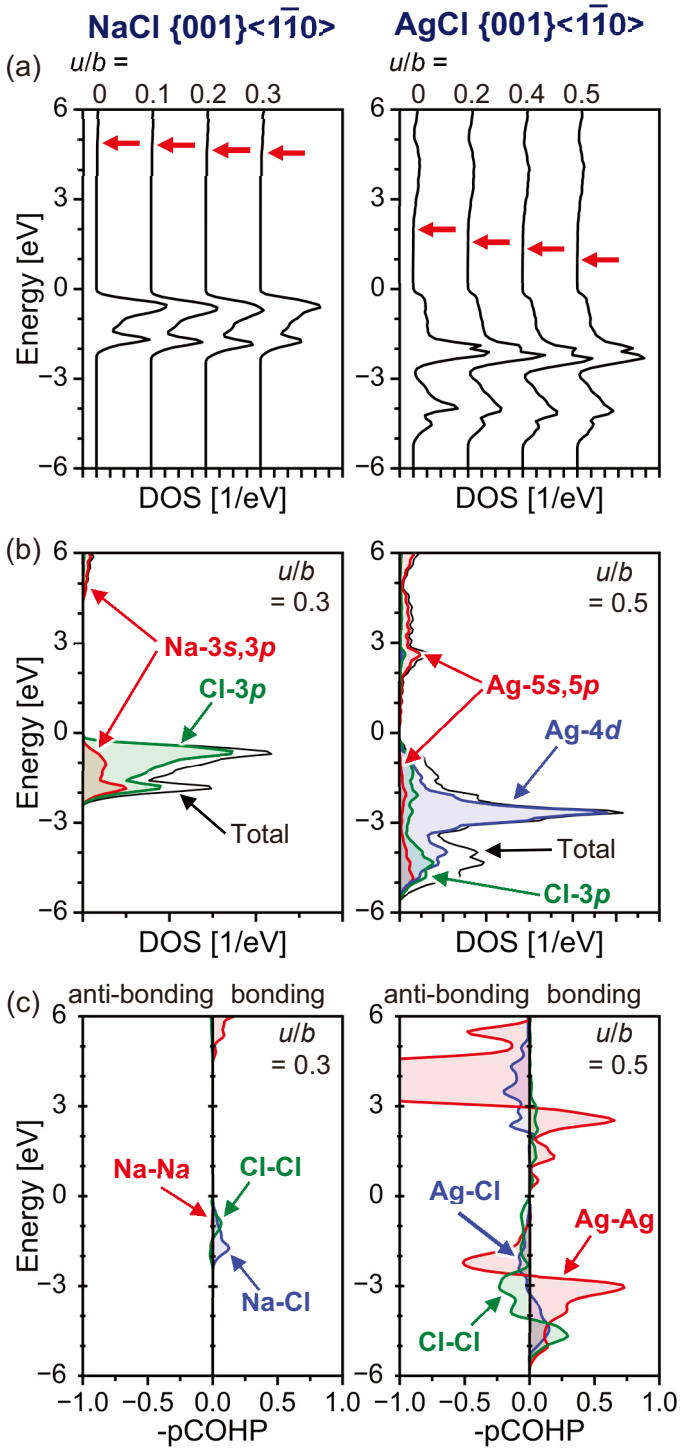

Figure 15. Electronic structures in the two atomic layers across the slip plane in {001}<110> slip of NaCl and AgCl. (a) Local DOS curves. Red arrows in the figure represent positions of the conduction-band bottoms. (b) Atomic-orbital components in the DOS curves at $u/|\vec{b}| = 0.3$ for NaCl and at $u/|\vec{b}| = 0.5$ for AgCl. (c) –pCOHP profiles at $u/|\vec{b}| = 0.3$ for NaCl and at $u/|\vec{b}| = 0.5$ for AgCl.

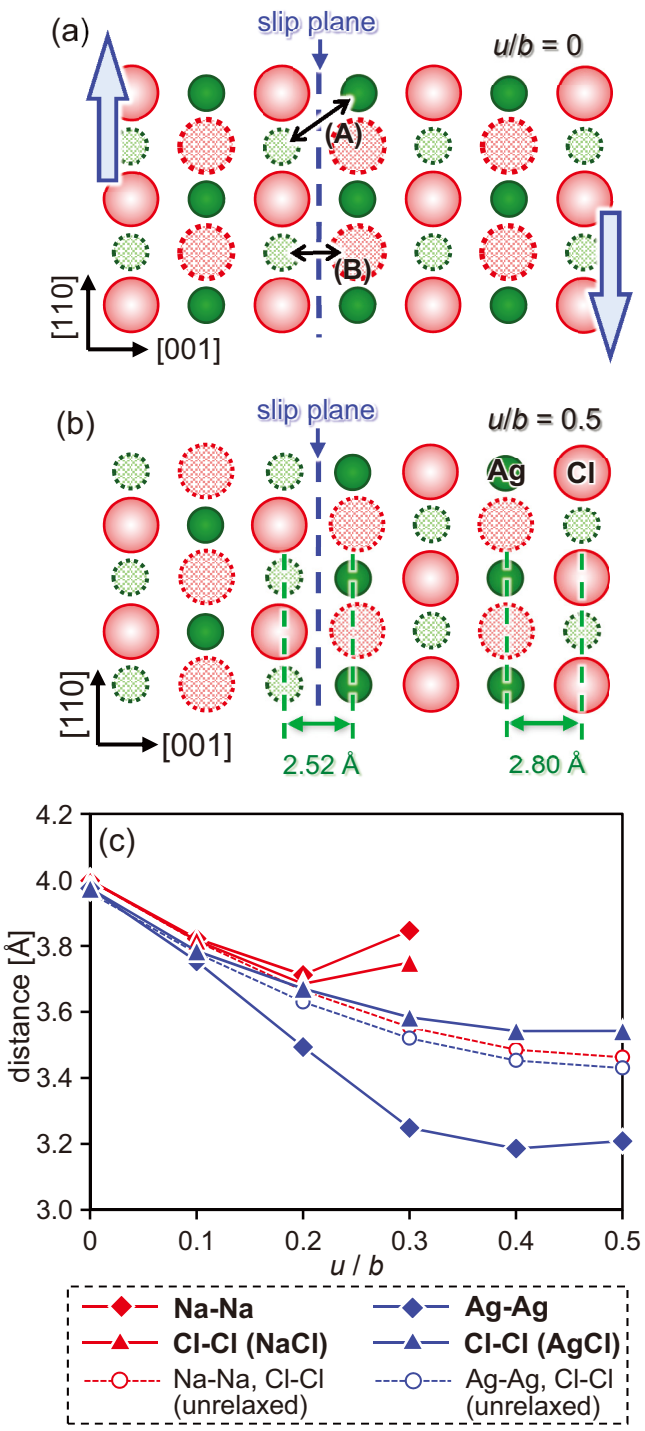

Figure 16. Schematic illustrations of atomic arrangements in the {001}<110> slip, viewed along the slip plane. (a) $u/|\vec{b}| = 0.0$, and (b) $u/|\vec{b}| = 0.5$ (with relaxation). These are drawn in the same manner with Figs. 7, 10 and 13. Interionic distances for the type-A pairs in NaCl and AgCl as a function of $u/|\vec{b}|$ are shown in (c).

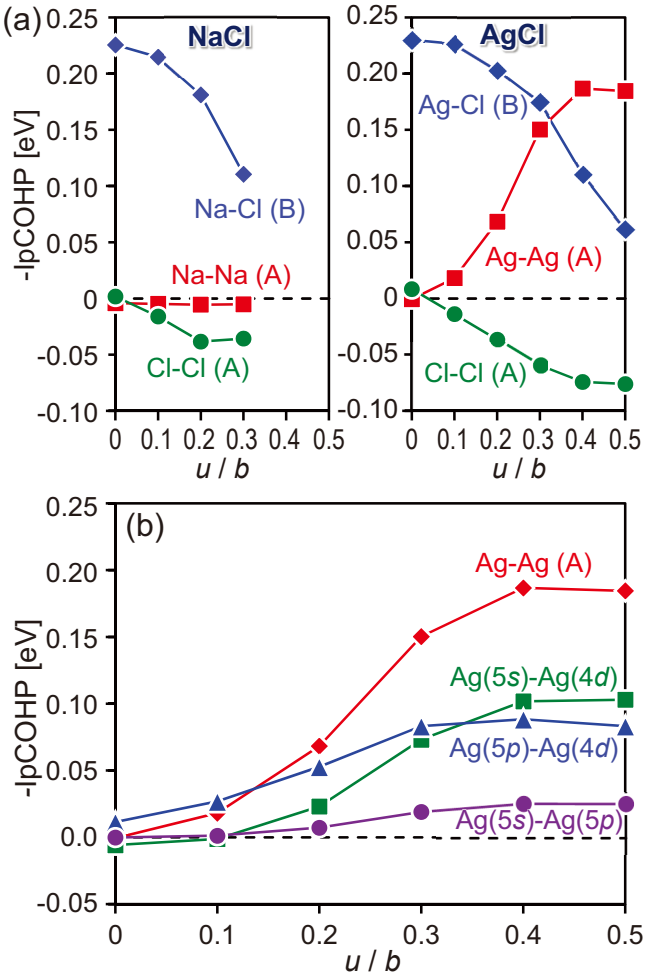

Figure 17. (a) –IpCOHP values of ionic pairs across the slip plane in the {001}<110> slip as a function of $u/|\vec{b}|$. (b) Atomic-orbital resolved –IpCOHP values for the type-A Ag-Ag pair.

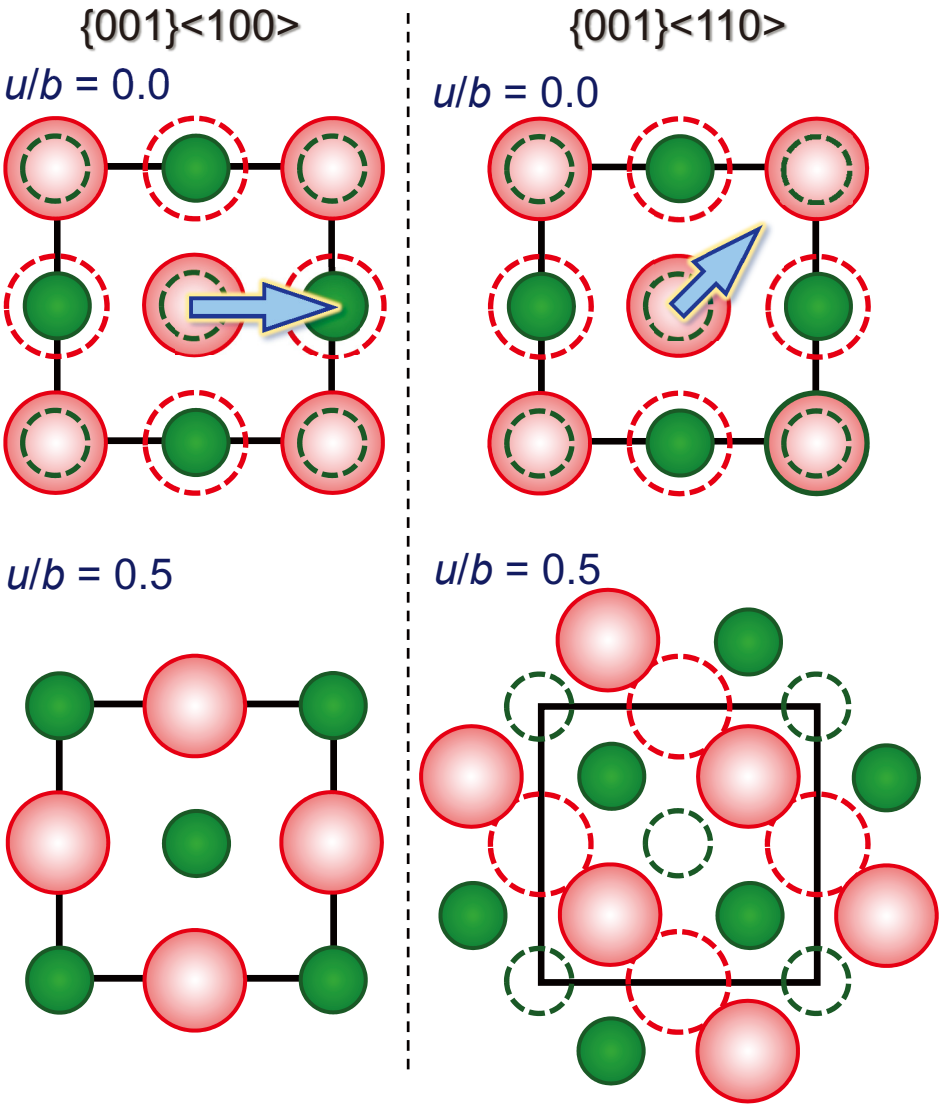

Figure 18. Illustrations of atomic configurations viewed normal to the slip plane for the {001}<100> and {001}<110> slip systems. Small and large dotted circles display cations and anions located below the slip plane. Upper figures are those before shear displacement, while lower ones after displacement of $u/|\vec{b}| = 0.5$.